Biosensors and Bioelectronics 87 (2017) 686–692

Contents lists available at ScienceDirect

Biosensors and Bioelectronics

journal homepage: www.elsevier.com/locate/bios

A multichannel smartphone optical biosensor for high-throughput point-of-care diagnostics

Li-Ju Wang, Yu-Chung Chang, Rongrong Sun, Lei Li *

School of Mechanical and Materials Engineering, Washington State University, Pullman, WA, 99164 USA

ARTICLE INFO

Article history:
Received 8 July 2016
Received in revised form
6 September 2016
Accepted 7 September 2016
Available online 9 September 2016

Keywords:
Optical biosensor
Smartphone spectrometer
High-throughput diagnostics
Protein detection
Immunoassay
Point-of-care

ABSTRACT

Current reported smartphone spectrometers are only used to monitor or measure one sample at a time. For the first time, we demonstrate a multichannel smartphone spectrometer (MSS) as an optical biosensor that can simultaneously optical sense multiple samples. In this work, we developed a novel method to achieve the multichannel optical spectral sensing with nanometer resolution on a smartphone. A 3D printed cradle held the smartphone integrated with optical components. This optical sensor performed accurate and reliable spectral measurements by optical intensity changes at specific wavelength or optical spectral shifts. A custom smartphone multi-view App was developed to control the optical sensing parameters and to align each sample to the corresponding channel. The captured images were converted to the transmission spectra in the visible wavelength range from 400 nm to 700 nm with the high resolution of 0.2521 nm per pixel. We validated the performance of this MSS via measuring the concentrations of protein and immunoassaying a type of human cancer biomarker. Compared to the standard laboratory instrument, the results sufficiently showed that this MSS can achieve the comparative analysis detection limits, accuracy and sensitivity. We envision that this multichannel smartphone optical biosensor will be useful in high-throughput point-of-care diagnostics with its minimizing size, light weight, low cost and data transmission function.

1. Introduction

To fill the translational gaps in bringing biodetection technologies from central laboratories to field and clinics (Kost et al., 1999), point-of-care testing (POCT) is booming in these years (Vashist et al., 2015; Holland and Kiechle, 2005). POCT allows patient diagnosis in the physician's office, an ambulance (Di Serio et al., 2006), or the emergency department (Fermann and Suyama, 2002), and pathogen/viruses biodetection in-field (Nichols, 2007; Vasoo et al., 2009). The timely results allow doctors to immediately treat patients. With the increase in the widespread smartphone popularity, mobile point-of-care technology (MPOCT) has shown promise in meeting the demand in remote and less-resource areas (Xu et al., 2015; Ozdalga et al., 2012). Most pocket-size smartphones are able to access the internet which makes real-time monitoring health conditions and transmitting diagnostic results online possible. Recently, MPOCT has drawn much attention in improving health delivery and in reforming the diagnostic paradigm, called m-Health (Steinhubl et al., 2015; Ventola, 2014; Erickson et al., 2014). M-Health is defined by the Global Observatory for e-health of World Health Organization (WHO) as "medical and public health practice supported by mobile devices, such as mobile phones, patient monitoring devices, personal digital assistants and other wireless devices" (WHO, 2001).

Spectroscopy is utilized in almost every field of science whenever electromagnetic radiation interacts with matter (Valeur and Brochon, 2012; Bakeev, 2010). Optical spectrum has been widely used as a diagnostic/detection method to characterize material amounts, properties, and components. Conventional laboratory optical spectral analyzers/readers, which have dedicated light splitting, guiding, and fitting mechanisms, and high sensitive light sensors, are normally very expensive and bulky. To deliver on-site biomedical diagnostics, there are tremendous needs in transition from laboratory testing to mobile diagnostic platforms. Much effort has been devoted for developing miniaturized smartphone spectrometers (Long et al., 2015). The three most common detection modalities of smartphone spectrometers are absorption (Wang et al., 2016; Guo et al., 2015; Long et al., 2014; Hu et al., 2015), fluorescence (Yu et al., 2014; Jiang et al., 2014), and photonic crystal based detection (Gallegos et al., 2013). These recently reported smartphone spectrometers have demonstrated that smartphone spectrometers with one detection modality can meet clinical requirements and have the potential to expand the use to environment assays in rural, remote, or low-resource areas.

* Corresponding author.
E-mail address: lei.li2@wsu.edu (L. Li).

http://dx.doi.org/10.1016/j.bios.2016.09.021
0956-5663/

Furthermore, two combined detection modalities in a smartphone spectrometer have been shown the feasibility (Hossain et al., 2015). However, all current reported smartphone spectrometers are single-channel detection. It means that only one sample can be monitored or measured in each measurement by these smartphone spectrometers. For on-site biomedical diagnostics or in-field testing, there are massive samples at the same time for analyzing. Therefore, both portable devices and high-throughput detection are critical issues. Single-channel smartphone spectrometers are portable, but far beyond the need for high-throughput detection. Moreover, most biomedical immunoassays or diagnostic tests are performed on the commonly used microtiter plates (microplates) for high-throughput testing. It is difficult to directly apply the reported single-channel smartphone spectrometers on the microplate-based assays in one step. For detecting microplate-based assays, Ozcan's group developed an optical-fiber-based cellphone microplate colorimetric reader for enzyme-linked immunosorbent assays (ELISA) (Berg et al., 2015). The data analysis was by extracting Red, Green and Blue channels in a digital image. No prior high-throughput multichannel smartphone spectrometers have been reported.

Here, we demonstrate a high sensitive multichannel smartphone spectrometer (MSS) as the optical biosensor for high-throughput point-of-care biomedical diagnostics. To achieve accurate multichannel optical sensing by a smartphone camera, two challenges need to be overcome. First, the limited field-of-view (FOV) unmatching problem between the smartphone camera and the samples leads to the optical aberration and incorrect analytical results. For example, an Apple iPhone 5 smartphone uses a 4.1 mm lens to provide a 33 mm equivalent FOV. On a 96-well microplate (85.5 mm × 127.8 mm), this small FOV can only view a few samples with nonuniform light distribution among these samples. Second, spectral crosstalk between neighboring channels in the multichannel spectrometer must be avoided. In this work, we designed a low-cost microprism array to enlarge the FOV of the smartphone sensor and to fit the FOV of a microplate. We utilized a backlight panel and a micro-aperture array to achieve uniform and isolated lighting distribution for each channel of the MSS to avoid the spectral crosstalk. Using the commercial 96-well microplate as the design model, we developed an 8-channel smartphone spectrometer as high-throughput optical biosensor for the first time. On the other hand, the detecting sensor of the smartphone camera is controlled by the smartphone's camera application (App) to automatically adjust optical parameters under different circumstances. To ensure the consistency in different circumstances, we developed an App to align each channel and to control the optical parameters related to optical sensing. To evaluate the performance of the MSS, we used the MSS to determine the concentrations of proteins, which are routine tests for diagnosing diseases or monitoring health and can only be conducted in diagnostic laboratories. We also assayed a clinical cancer biomarker in human serum for human disease diagnostics by the MSS. Both results measured by the MSS were compared with those read by a commercial laboratory spectrometer.

2. Material and methods

2.1. Light tilting principle, design and fabrication of the microprism array

To enlarge the FOV of the camera sensor, a microprism array was designed for tilting incident light from one column of a 96-well microplate. A prism can deviate the incident light to an deviation angle σ, as schematically shown in Fig. S1. The light ray-tracing can be calculated by Eq. (1):

$$\tan\frac{\sigma}{2} = \frac{\sin\frac{\delta}{2}}{\frac{n_{\text{prism}}}{n_0} - \cos\frac{\delta}{2}} \quad (1)$$

where δ is the angle of refraction (prism apex angle), $\boldsymbol{n_{\text{prism}}}$ is the refractive index of the prism material, and $\boldsymbol{n_0}$ is the refractive index of air. Based on the template of one column of a 96-well microplate, a microprism array was designed with different apex angles (δ) for each microprism to tilt light from different position to the smartphone camera sensor. First, an 8-channel microprism array for the first column was designed and then the array was repeated for a total of 12 rows in Fig. S2. In every column, the 8-channel microprism array is symmetric to the center and the apex angles (δ) and light deviation angles (σ) of each microprism are both indicated in Fig. S2. Since the camera sensor can detect light from the two central wells in each column of 96-well microplate clearly without light tilting, there were no microprisms in the middle two channels.

To fabricate the designed microprism array at low cost, we used a hybrid manufacturing process as illustrated in Fig. S3. In the first step, a negative mold of the microprism array was 3D printed (uPrint SE Plus, Stratasys, Eden Prairie, MN, USA) by using acrylonitrile-butadiene-styrene (ABSplus-P430, Stratasys, Eden Prairie, MN, USA). Next, to increase the resolution and the surface quality while molding the microprisms, one layer of a thermoplastic sheet (Polyethylene terephthalate, PET sheet, thickness 1/32 in., widgetworks, NY, USA) was vacuum coated on the surface of the negative mold by a compact vacuum forming machine (JT-8 Vacuum Forming Machine, China). After smoothing the surface of the negative mold, PDMS (SYLGARD® 184 silicone elastomer kit, base and curing agent mixed at a ratio 10:1, Dow Corning) was poured onto this PET-covered mold and fully cured at 60 °C for 2 h. A transparent microprism array was fabricated after peeling off.

2.2. Multichannel smartphone spectrometer system

Fig. 1(a) schematically shows the platform of the 8-channel smartphone spectrometer. An iPhone 5 (Apple, Inc., Cupertino, CA, USA) smartphone with a rear camera, which integrates an 8-megapixel backside-illuminated sensor (BIS) with 3264 × 2448 pixels, was used in the MSS. A diffractive grating (1200 grooves/mm, GT13–12, Thorlabs, USA) was utilized to generate diffractive spectra. The first order diffraction angle of this grating is 39.5° for green light. A 45° angle was designed between the optical axis of the incoming light and the normal direction of the grating. Thus, the first-order diffraction spectrum can be captured by a smartphone camera when the camera is directly put in contact with the grating. In order to reduce the cost and the total size, no extra lenses and small-diameter apertures were used in this design. We utilized the lenses in the smartphone camera to directly focus the spectrum.

A smartphone holder for an iPhone 5 was designed to hold both the smartphone and the diffractive grating. A smartphone support was designed to keep a minimal distance between the grating and the microplate. The distance from the grating to the top surface of the microplate was about 90 mm. The smartphone supporter was also functioned as a slit aperture which only allows light from one column to reach the grating to avoid interfere of light from different columns. In the bottom part of the MSS, a microplate holder was designed to hold all the other components. These components included a low-cost backlight panel (112 mm × 88 mm × 3 mm), one aperture array with aperture diameter 6 mm that placed between the backlight panel and the microplate, a microplate that can slide in and out of the holder from one side, and another aperture array with aperture diameter 4 mm that placed above the microplate. The microplate was placed

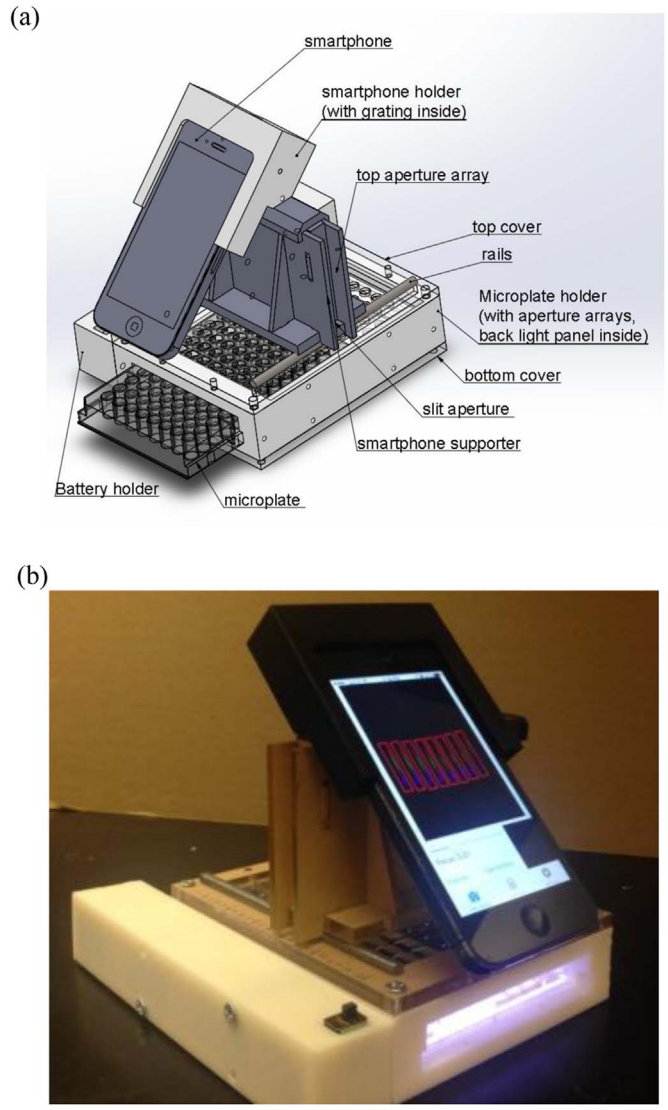

Fig. 1. (a) The 3D model and (b) the assembled setup of the 8-channel smartphone spectrometer. (c) The screenshot of the App in the first view to align each spectrum into each channel, adjust focus, and take photos. (d) The screenshot of the App in the second view to control the optical sensing parameters. (For interpretation of the references to color in this figure, the reader is referred to the web version of this article.)

between the two aperture arrays and these three components were in precise alignment so that illumination light only passed through microwells and the areas between wells were all blocked. The spectral crosstalk can be perfectly avoided. To user-friendly scan samples from one column to the next column of the 96-well microplate, two sliding rails were designed on the top of the top cover. The smartphone supporter can slide along these two rails to every column of the 96-well microplate.

On top of the top aperture array, the PDMS microprism array was integrated and aligned with the aperture array to tilt light into the FOV of a smartphone camera. The backlight panel and the two aperture arrays were glued inside the microplate holder. The microprism array was hold tightly by a top cover lid. Three 9 V batteries were used to power the backlight panel and one battery holder with a switch was designed and placed at one side of the microplate holder. Two light sources were prepared for this MSS. The first light source is 8 micro Xenon bulbs (1-Cell AAA, Maglite, Ontario, CA, USA) as the white light source, and the second light source is 8 compact white light-emitting diodes (LED). All light sources were incident from one side of the backlight panel. Light can be reflected multiple times inside the backlight panel and exited from the top of the panel with a uniform light distribution.

The smartphone holder, the microplate holder, and the battery holder were 3D printed using opaque ABS. The smartphone supporter was made by gluing 7 pieces of laser-cut acrylic sheets (1/16 in. thick). All sides of the supporter were covered by opaque protection paper to block stray light. The height of the smartphone supporter, i.e. the distance from the camera to the top of the microplate, was 90 mm. The bottom aperture array with aperture diameter 6 mm and the top aperture array with aperture diameter 4 mm were made by laser cutting a piece of the transparent acrylic sheet (1/32 in. thick) and painted to black. The top cover lid was also laser cut of an acrylic sheet (1/16 in. thick). Two 1/8 in. stainless steel rods as the sliding rails were glued on two slots that laser-cut on the top cover lid. The assembled MSS with an iPhone 5 smartphone was shown in Fig. 1(b).

2.3. Digital image acquisition and data processing

An iPhone mobile multi-view App was developed using the Swift programming langue (Apple Inc, Cupertino, California, U.S.) to control the optical sensing parameters and to align the spectrum in each channel. The first view in Fig. S4 was used to align each spectrum with the smartphone camera sensor by 8 square frames in 8 channels, respectively. In addition, the first view can review spectrum, adjust focus by changing the “Focus” slide bar, and take images by tapping the “Take photos” button. 5 pictures were captured in sequence to minimize the possible small intensity fluctuations which arose from the light source and the camera sensor. Then, the app automatically saved captured pictures to the image gallery. The second view in Fig. S5 can adjust exposure time, ISO value, and white balance. The consistent optical parameters were set for all measurements. To process and analyze spectral data, a Matlab (Mathworks, Natick, MA, USA) graphical user interface (GUI) program was developed. First, the program transformed the corresponding pixel values to the specific wavelength values that were measured in the light calibration step. Then, 5 pictures of each sample were imported to read the average optical intensity in each channel. The average of 60 spectral lines of each spectrum was calculated to obtain average light intensity vs. wavelength. Finally, the program processed the transmission and absorbance spectrum to determine the concentrations of the analyte. For future cloud-based computation, this program can be installed in a central server. The smartphone App can wirelessly transmit the obtained images to the central server, receive and display the results directly on the smartphone.

2.4. Quantification of protein

Quantifying the amount of protein, also known as quantitative proteomics, is a very important and common assay in biochemistry research and clinic diagnostics (Noble and Bailey, 2009; Stoscheck, 1990). By determining the amount of protein, the diseased and healthy patients can be diagnosed. For example, protein in urine, referred to proteinuria, is suggestive of kidney diseases or infection, and is especially important for pregnant woman (Price et al., 2005). A Bradford assay kit (Thermo Scientific, Waltham, MA, USA) was purchased to determine protein concentration. The Bradford protein assay utilizes Coomassie Brilliant Blue G-250 colloidal dye to quantify the amount of protein. In the acidic condition, protein binds to the dye molecules to form a protein-dye complex. The protein-dye complex leads to a spectral shift from the brown form of the dye (absorbance maximum at a wavelength of 465 nm) to the blue form of the dye (absorbance maximum at a wavelength of 595 nm).

We prepared two sets of serially diluted bovine serum albumin (BSA) standards in 0.01 M phosphate buffered solution (PBS, pH 7.4), including the set in the high concentration range from 0.125 mg/mL to 1.5 mg/mL, and that in the low concentration range from 2 μg/mL to 25 μg/mL. A blank sample was prepared as 0 mg/mL BSA in PBS. Assaying high concentrations of BSA, 10 μL of each BSA standard was added into the appropriate microplate wells. 300 μL of G-520 colloidal dye was then added to each well. To detect the low concentrations of BSA, 150 μL of each BSA standard was mixed with 150 μL of G-520 dye in each well. After gentle tapping the microplate for 30 s and developing for 10 min, it was ready to read the results by both the MSS and a laboratory instrument (Tecan Safire2, Männedorf, Switzerland) for two replicates.

2.5. Cancer biomarker immunoassays

Human Interleukin-6 (IL-6) has been extensively shown to be a relevant cancer biomarker for lung (Brichory et al., 2001; Yanagawa et al., 1995), prostate (Michalaki et al., 2004; Giri et al., 2001), liver (Park et al., 2010; Naugler et al., 2007), breast (Knüpfer and Preiß, 2007; Sullivan et al., 2009), and epithelial cancers (Schafer and Brugge, 2007). Accurately evaluating the expression of IL-6 in human serum has been considered to track, classify, and prognose various cancers. An enzyme-linked immunosorbent assay (ELISA) kit was purchased (Invitrogen, Camarillo, CA, USA) to measure IL-6 levels in human serum. Lyophilized IL-6 was reconstituted in the standard diluents, and serially diluted from 2 pg/mL to 250 pg/mL. 50 μL of each serially diluted IL-6 standard was added to each microwell which was pre-coated with human IL-6 capture antibodies. The blank well was incubated with 0 pg/mL of IL-6. Then 50 μL of detection antibody (biotinylated antibody) was added to each well. The solutions were carefully covered for 2-h incubation at room temperature. Next, the solutions were removed, and each well was washed 4 times with the wash buffer. 100 μL of Streptavidin-HRP solution was added to each well followed by incubation for another 30 min, and the wash steps were repeated again. 100 μL of chromogen solution (TMB substrate) was then added to each well. After developing for 30 min in dark at the room temperature, 100 μL of stop solution was added to stop the reaction. The immunoassay results were ready to measure the absorbance at a wavelength of 450 nm by both the MSS and the laboratory instrument (Tecan Safire2, Männedorf, Switzerland) for two replicates.

3. Results and discussion

3.1. Wavelength calibration of the multichannel smartphone spectrometer

We calibrated two types of light sources including the white light (Xenon bulbs) and the LED, respectively. Because the MSS was well assembled, we were not able to insert laser light sources to directly calibrate the correlated pixel values with the wavelength. We used an indirect calibration method to map the pixel-to-wavelength relationship. First, we utilized a published handheld smartphone single-channel spectrometer to calibrate the mapping of pixel to wavelength (Wang et al., 2016). One Helium-Neon (HeNe) laser (632.8 nm, Melles Griot, NY, USA) and three laser diodes (405 nm, 530 nm, and 650 nm wavelength) were applied to calibrate the pixel-wavelength mapping in Fig. S6. The wavelength resolution is 0.2521 nm/pixel. Next, we respectively obtained the spectrum distribution of the white light and the LED that were respectively applied in the MSS in Fig. S7. By comparing the pixel-wavelength mapping obtained on the single-channel smartphone spectrometer (Wang et al., 2016) and the spectrum obtained directly from this MSS, we identified the correlated pixels to wavelengths in the MSS and also determined the positions of the 8 alignment frames for 8 channels.

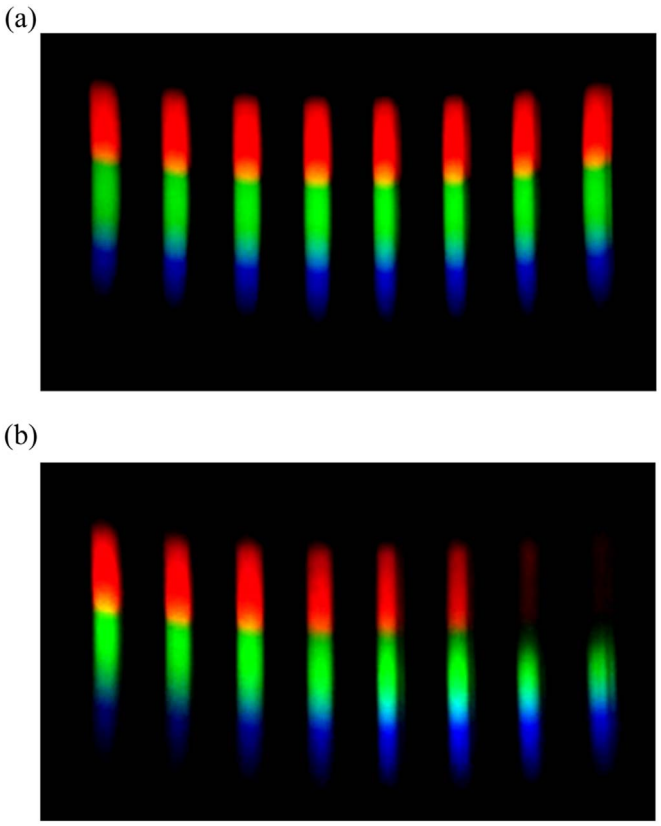

Fig. 2. The 8-channel transmission spectral images of (a) DI water and (b) serial diluted BSA standards in the high concentration ranges (0.125–1.5 mg/mL) with the blank sample (0 mg/mL BSA).

3.2. Protein quantification by the multichannel smartphone spectrometer

To validate the performance of the MSS using a white light source, Fig. 2 presents the 8-channel transmission spectra and the absorption spectra of BSA in the high concentration working range measured by the MSS and the laboratory instrument, respectively. The full visible spectra from 400 nm to 700 nm were readout by the MSS and the lab instrument. The 8-channel transmission spectral images of DI water and the high concentrations of BSA are shown in Figs. 2(a) and (b). It can be seen that DI water has no absorbance to visible light while the different concentrations of BSA mixed with G-520 reagent have red-light absorbance.

The absorption spectra of the high concentrations of BSA standards (0.125–1.5 mg/mL) and the blank sample (0 mg/mL of BSA) measured by the MSS and the lab instrument are presented in Figs. 3(a) and (b), respectively. In clinical chemistry, the isosbestic point is the indicator to verify the accuracy in the wavelength of the spectrometer, as the quality assurance method, relying on the total absorbance of the sample fixing during chemical reactions at the isosbestic point. At the wavelength of 525 nm, there is an isosbestic point in both spectra read by the MSS and the lab instrument in Figs. 3(a) and (b), respectively. It is strongly indicated that the high accuracy of pixel-wavelength mapping of the MSS by the indirect wavelength calibration method compared with the results from the lab instrument. With increasing the concentrations of BSA, the absorption spectrum experiences a

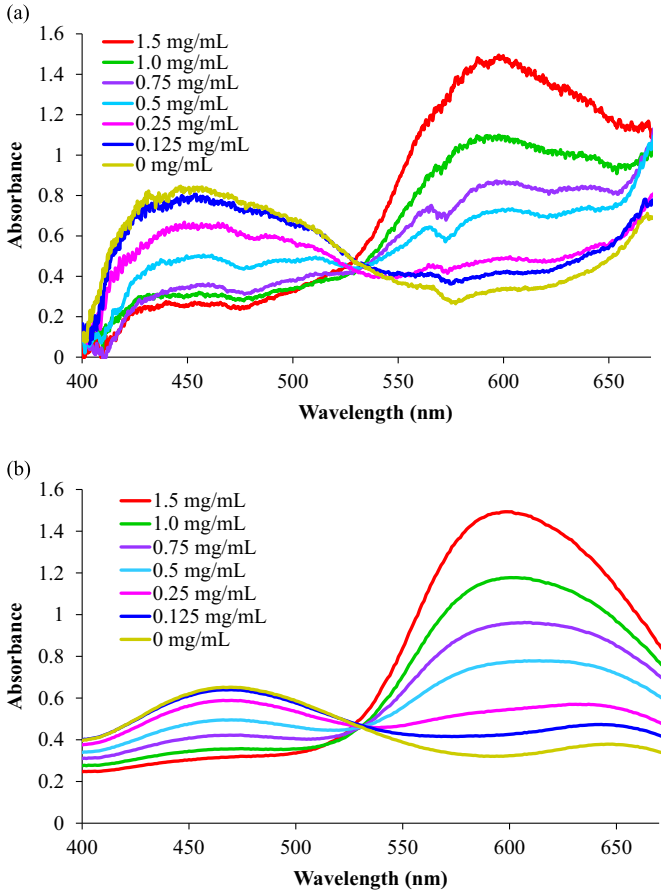

Fig. 3. The absorption spectra of serial diluted BSA standards in the high concentration ranges (0.125–1.5 mg/mL) with the blank sample (0 mg/mL BSA) read by (a) the MSS and (b) the laboratory instrument.

redshift and the absorption peak is at the wavelength of 595 nm.

In the first set of the high concentrations (0.12–1.5 mg/mL), the linear calibration plot of absorbance vs. the concentrations of BSA measured by the MSS and the lab instrument is presented in Figs. 4(a) and (b), respectively. The linear correlation (R^2) achieved 0.9977 by the MSS to quantify the BSA concentrations which was comparative to the results by the lab instrument (R^2=0.9952). The limit of detection (LOD) was calculated as three standard deviations above the absorbance of blank sample (0 mg/mL of BSA) measured by the MSS and the laboratory instrument, respectively. The MSS achieved an LOD of 0.187 mg/mL which was at the same level of the LOD of the lab instrument (0.240 mg/mL). To specifically assess the agreement between the two instruments, the linear correlation between the MSS and the lab instrument showed the strongly agreement with each other (R^2=0.9927) in Fig. 4(c).

The assay of the low concentrations (2–25 μg/mL) were evaluated in Figs. 5(a) and (b) which was more challenging than determining the high concentrations of protein due to the requirement of the high sensitivity of the MSS. The linear regression analysis showed that the MSS can perform precision measurements of protein quantification in the low concentration range (R^2=0.9953) which was comparative to the lab instrument (R^2=0.9910). The LOD measured by the MSS was 4.4 μg/mL and it is comparative with the LOD measured by the lab instrument (4.1 μg/mL). The linear correlation (R^2=0.9847) between the two instruments in Fig. 5(c) evidently demonstrated the highly agreement in the measurement results by both instruments. In addition, the intensity of the white light illuminating the high

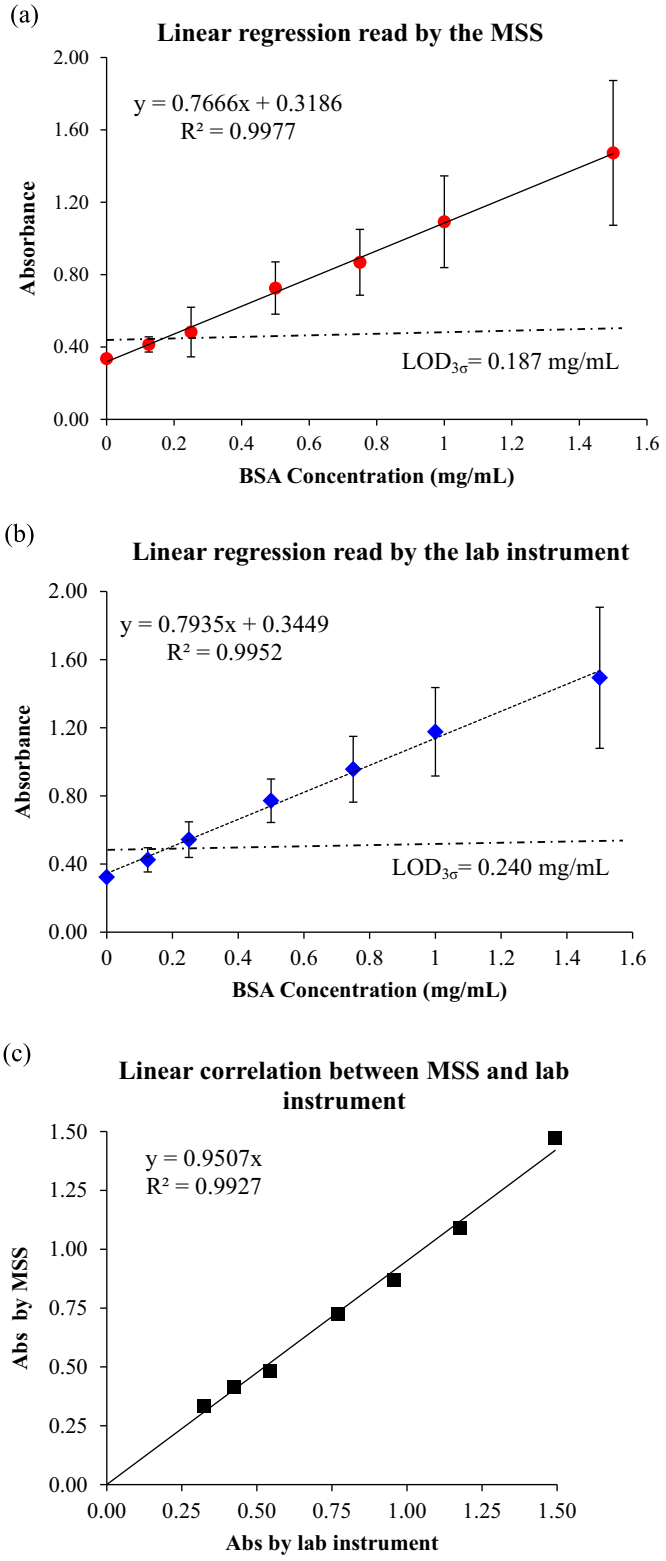

Fig. 4. (a) The linear regression between the absorbance at 595 nm and the BSA concentration measured by the MSS, and (b) by the laboratory instrument in the high concentration range (0.125–1.5 mg/mL). (c) The linear correlation between the absorbance results measured by the MSS and the laboratory instrument.

concentrations of protein samples by the MSS was slightly weaker (0.9507 fold) than the light intensity of the compared lab instrument in Fig. 4(c), and that illuminating the low concentrations of protein samples by the MSS was slightly stronger (1.0387 fold) than the light intensity of the compared lab instrument in Fig. 5(c).

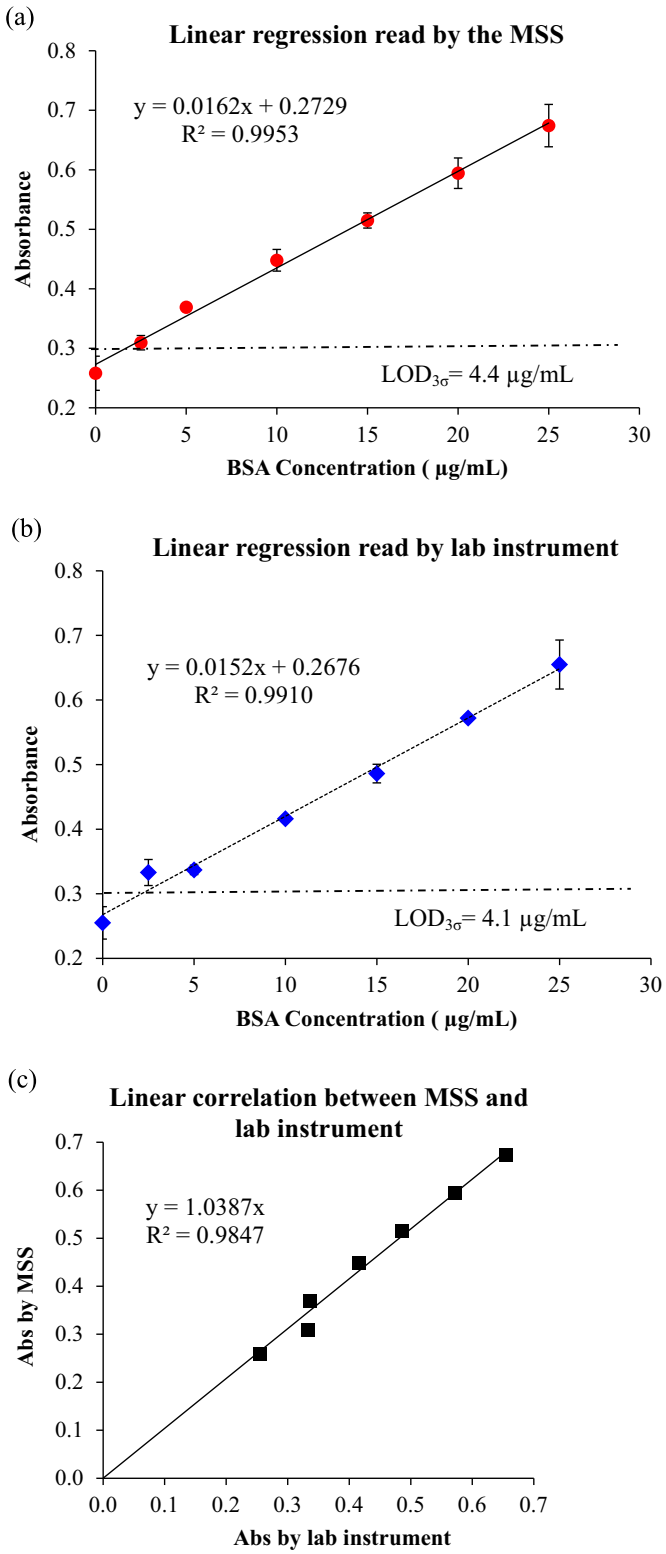

Fig. 5. (a) The linear regression between the absorbance at 595 nm and the BSA concentration measured by the MSS, and (b) by the laboratory instrument in the low concentration range (2–2 μg/mL) (c) The linear correlation between the absorbance results measured by the MSS and the laboratory instrument.

Since different instruments have differences in the illumination intensity and sensor sensitivity, the comparison in the light intensity can be used as the reference factors while comparing to different instruments in the future. The capability of the MSS for quantifying protein from 2 μg/mL to 1.5 mg/mL has been validated

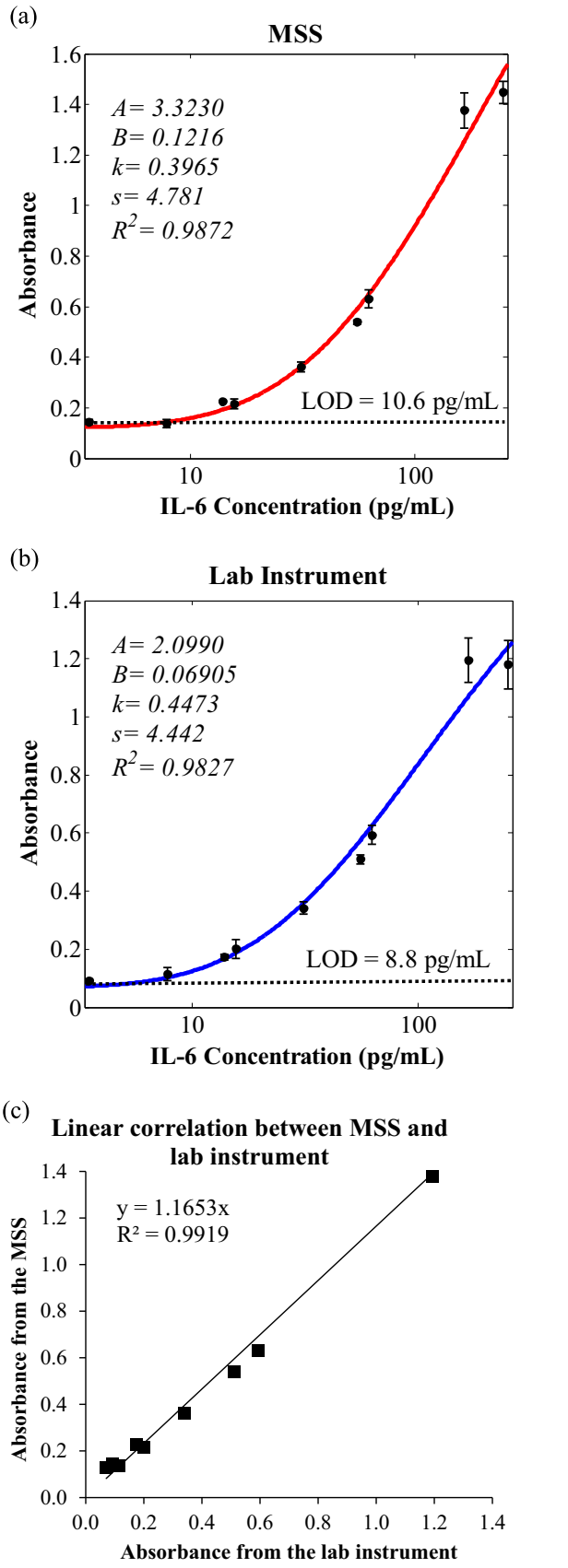

Fig. 6. The dose-response fitting curves for IL-6 concentrations in human serum measured by (a) the MSS and (b) the laboratory instrument. (c) The linear correlation between the MSS and the lab instrument.

with high accuracy compared with the lab instrument. At the same time, the MSS showed the high sensitivity to measure the low concentrations of the protein.

3.3. Immunoassaying cancer biomarker measured by the multichannel smartphone spectrometer

Next, we evaluated the ability of the MSS using a LED source to high-throughput measure IL-6 concentration in human serum. The completed immunoassays were read at the wavelength of 450 nm. The absorbance is a function of IL-6 concentrations fitted by the sigmoidal curve (dose-response curve), governed by Eq. (2):

$$f(x) = A + \frac{B - A}{1+(kx)^s} \quad (2)$$

where A and B are the y-axis maximum and minimum asymptote. k is the inflection point. x represents $\log_{10}[\text{IL-6}]$ and s is the Hill's Slope to describe the steepness of the fitting curves. The LOD was calculated as three standard deviations above the absorbance of blank sample (0 pg/mL of IL-6 in human serum) measured by the MSS and the laboratory instrument, respectively. In Figs. 6(a) and (b), the dose-response curves with 4 parameters (A, B, k, and s) are presented. The goodness-of-fit (R^2) of the dose-response fitting immunoassaying curve measured by the MSS achieved to 0.9872 which was highly comparative to the performance of the lab instrument ($R^2=0.9827$). The MSS achieved an LOD of 10.6 pg/mL which was at the same level of the LOD by the lab instrument (8.8 pg/mL). It provided the strong evidence that the sensitivity of the MSS using the LED backlight achieved the clinical diagnostic requirement. Furthermore, the intensity of the LED backlight illuminating the biomarker IL-6 in human serum by the MSS was slightly stronger (1.1653 fold) than the light intensity of the lab instrument in Fig. 6(c) with the high agreement ($R^2=0.9919$) in the results of the two instruments. By assessing IL-6 immunoassaying, the MSS using the LED backlight was successfully demonstrated the high accuracy and the high sensitivity compared with the lab instrument.

4. Conclusions

In this work, we first-time developed a portable multichannel smartphone spectrometer (MSS) as the high-throughput optical biosensor by integrating a custom-designed microprism array for point-of-care diagnostics. The wavelength resolution of the MSS is 0.2521 nm/pixel. We illustrated the performance of the MSS by quantifying protein concentrations and immunoassaying a cancer biomarker that are both essentially important in disease clinic diagnosis and biomedical research. First, the linearity results of quantifying proteins showed the good correlation in the high concentration range ($R^2=0.9927$) and the low concentration range ($R^2=0.9847$) between the MSS and the laboratory instrument. The sensitivity of the MSS was also evaluated by its capability of measuring the very low concentration of protein (2 μg/mL). Second, the cancer biomarker was immunoassayed and curve-fitted by the dose-response sigmoidal model which is the most common model in clinical chemistry. The agreement was highly correlated ($R^2=0.9919$) between the MSS and the lab instrument. Moreover, the comparative LOD (10.6 pg/mL) of the MSS satisfied the clinical requirements. These two sets of tests provided strong evidences that the MSS can perform the high-throughput point-of-care diagnostics with the validated high sensitivity and accuracy. Such high performance of the MSS was contributed by the microprism array to navigate the light from each sample to each channel and the micro-aperture array to avoid the spectral crosstalk between each channel. Considering the affordability, we invented a hybrid manufacturing process to fabricate the low-cost PDMS microprism array. Using 3D printed accessories and the affordable hybrid manufacturing process for the PDMS microprism array, the MSS only costs less than $150 USD. Thus, this affordable MSS opens a promising avenue toward in-field high-throughput point-of-care diagnostics by multichannel optical detection on the smartphone.

Acknowledgments

The authors would like to acknowledge and thank Frank Innovation Zone of Washington State University for helping 3D printing and laser cutting.

Appendix A. Supporting information

Supplementary data associated with this article can be found in the online version at doi:10.1016/j.bios.2016.09.021.

References

Bakeev, K.A., 2010. Process Analytical Technology: Spectroscopic Tools and Implementation Strategies for the Chemical and Pharmaceutical Industries. John Wiley and Sons, Hoboken, NJ, USA.
Berg, B., Cortazar, B., Tseng, D., Ozkan, H., Feng, S., Wei, Q., Chan, R.Y., Burbano, J., Farooqui, Q., Lewinski, M., Di Carlo, D., 2015. ACS Nano 9, 7857–7866.
Brichory, F.M., Misek, D.E., Yim, A.M., Krause, M.C., Giordano, T.J., Beer, D.G., Hanash, S.M., 2001. Proc. Natl. Acad. Soc. 98, 9824–9829.
Di Serio, F., Lovero, R., Leone, M., De Sario, R., Ruggieri, V., Varraso, L., Pansini, N., 2006. Clin. Chem. Lab. Med 44, 768–773.
Erickson, D., O'Dell, D., Jiang, L., Oncescu, V., Gumus, A., Lee, S., Mancuso, M., Mehta, S., 2014. Lab Chip 14, 3159–3164.
Fermann, G.J., Suyama, J., 2002. J. Emerg. Med. 22, 393–404.
Gallegos, D., Long, K.D., Yu, H., Clark, P.P., Lin, Y., George, S., Nath, P., Cunningham, B. T., 2013. Lab Chip 13, 2124–2132.
Giri, D., Ozen, M., Ittmann, M., 2001. Am. J. Pathol. 159, 2159–2165.
Guo, T., Patnaik, R., Kuhlmann, K., Rai, A.J., Sia, S.K., 2015. Lab Chip 15, 3514–3520.
Holland, C.A., Kiechle, F.L., 2005. Curr. Opin. Microbiol. 8, 504–509.
Hossain, M.A., Canning, J., Ast, S., Cook, K., Rutledge, P.J., Jamalipour, A., 2015. Opt. Lett. 40, 1737–1740.
Hu, P., Chen, Y., Snokusale, S., 2015. IEEE Virtual Conf. Appl. Commer. Sens., 1–5.
Jiang, L., Mancuso, M., Lu, Z., Akar, G., Cesarman, E., Erickson, D., 2014. Sci. Rep. 4, 4137.
Knüpfer, H., Preiß, R., 2007. Breast Cancer Res. Treat. 102, 129–135.
Kost, G.J., Ehrmeyer, S.S., Chernow, B., Winkelman, J.W., 1999. Chest 115, 1140.
Long, K.D., Yu, H., Cunningham, B.T., 2014. Opt. Express 5, 3792–3806.
Long, K.D., Yu, H., Cunningham, B.T., 2015. Proc. SPIE, 94820J-94820J..
Michalaki, V., Syrigos, K., Charles, P., Waxman, J., 2004. Br. J. Cancer 90, 2312–2316.
Naugler, W.E., Sakurai, T., Kim, S., Maeda, S., Kim, K., Elsharkawy, A.M., Karin, M., 2007. Science 317, 121–124.
Nichols, J.H., 2007. Clin. Lab. Med. 27, 893–908.
Noble, J.E., Bailey, M.J., 2009. Method Enzymol. 463, 73–95.
Ozdalga, E., Ozdalga, A., Ahuja, N., 2012. J. Med. Internet Res. 14, e128.
Park, E.J., Lee, J.H., Yu, G.Y., He, G., Ali, S.R., Holzer, R.G., Österreicher, C.H., Takahashi, H., Karin, M., 2010. Cell 140, 197–208.
Price, C.P., Newall, R.G., Boyd, J.C., 2005. Clin. Chem. 51, 1577–1586.
Schafer, Z.T., Brugge, J.S., 2007. J. Clin. Invest. 117, 3660–3663.
Steinhubl, S.R., Muse, E.D., Topol, E.J., 2015. Sci. Transl. Med. 7, 283v3-283rv3.
Stoscheck, C.M., 1990. Method Enzymol. 182, 50–68.
Sullivan, N.J., Sasser, A.K., Axel, A., Vesuna, F., Raman, V., Ramirez, N., Oberyszyn, T. M., Hall, B.M., 2009. Oncogene 28, 2940–2947.
Valeur, B., Brochon, J.C., 2012. New Trends in Fluorescence Spectroscopy: Applications to Chemical and Life Science. Springer Science and Business Media, Berlin, Germany.
Vashist, S.K., Luppa, P.B., Yeo, L.Y., Ozcan, A., Luong, J.H., 2015. Trends Biotechnol. 33, 692–705.
Vasoo, S., Stevens, J., Singh, K., 2009. Clin. Infect. Dis. 49, 1090–1093.
Ventola, C.L., 2014. Pharmacol. Ther. 39, 356.
Wang, L.J., Chang, Y.C., Ge, X., Osmanson, A.T., Du, D., Lin, Y., Li, L., 2016. ACS Sens. 1, 366–373.
World Health Organization (WHO) mHealth, 2001. New Horizons for Health through Mobile Technologies: Based on the Findings of the Second Global Survey on eHealth. Global Observatory for eHealth Series. 3. WHO, Geneva.
Xu, X., Akay, A., Wei, H., Wang, S., Pingguan-Murphy, B., Erlandsson, B.E., Li, X., Lee, W., Hu, J., Wang, L., Xu, F., 2015. Proc. IEEE 103, 236–247.
Yanagawa, H., Sone, S., Takahashi, Y., Haku, T., Yano, S., Shinohara, T., Ogura, T., 1995. Br. J. Cancer 71, 1095.
Yu, H., Tan, Y., Cunningham, B.T., 2014. Anal. Chem. 86, 8805–8813.